An adaptive approach for prediction of propellant feedline dynamics in fluid network

Sivaguru S. Ravindran
Department of Mathematical Sciences, University of Alabama in Huntsville, Huntsville, Alabama, USA, and

Alok K. Majumdar
Department of Propulsion System, NASA Marshall Space Flight Center, Huntsville, Alabama, USA

Received 19 April 2017
Revised 14 July 2017
15 July 2017
Accepted 26 July 2017

Abstract

Purpose – This paper aims to propose an adaptive unstructured finite volume procedure for efficient prediction of propellant feedline dynamics in fluid network.

Design/methodology/approach – The adaptive strategy is based on feedback control of errors defined by changes in key variables in two subsequent time steps.

Findings – As an evaluation of the proposed approach, two feedline dynamics problems are formulated and solved. First problem involves prediction of pressure surges in a pipeline that has entrapped air and the second is a conjugate heat transfer problem involving prediction of chill down of cryogenic transfer line. Numerical predictions with the adaptive strategy are compared with available experimental data and are found to be in good agreement. The adaptive strategy is found to be efficient and robust for predicting feedline dynamics in flow network at reduced CPU time.

Originality/value – This study uses an adaptive reduced-order network modeling approach for fluid network.

Keywords Adaptive algorithm, Network fluid system, Thermo fluid analysis, Unstructured finite volume method

Paper type Research paper

Nomenclature

A = cross-sectional area, ft^2;
C_f = specific heat of the fluid, Btu/lb °F;
C_L = flow coefficient;
C_p = specific heat at constant pressure, Btu/lb °F;
D = diameter of the pipe, ft;
f^* = Darcy–Weisback friction factor;
g_c = gravitational constant, 32.174 lb-ft/lb_f.s^2;
h = enthalpy, Btu/lb;
h_c = heat transfer coefficient, Btu/ft^2–s °F;

The work of S.S. Ravindran was supported in part by NASA grant #NNM16AA06A. This author was also supported in part by a grant from NASA Tech Excellence Program. The part of the work was conducted at Marshall Space Flight Center, Huntsville, Alabama, in the ER43/Thermal Analysis Branch. The authors would like to thank the Thermal Analysis Branch for their support.

International Journal of Numerical Methods for Heat & Fluid Flow
Vol. 28 No. 6, 2018
pp. 1335-1351

0961-5539
DOI 10.1108/HFF-04-2017-0162

J = mechanical equivalent of heat, equal to 778 ft-lb_f/Btu;
K_{f^*} = flow resistance coefficient, lb_f-s^2/(lb-ft)^2;
K_{rot} = non dimensional rotating flow resistance coefficient;
k = thermal conductivity, Btu/(ft-s °F);
k_p, k_I, k_D = feedback gain parameters;
L = length of the tube, ft;
L_g = initial length of air column in the pipe;
L_l = initial length for the water volume in the pipe;
L_T = initial total length of liquid and air column; $L_g + L_l$;
$\dot{m}$ = mass flow rate, lb/s;
m = resident mass, lb;
Nu = Nusselt number;
Pr = Prandtl number;
Re = Reynolds number;
n = number of branches;
p = pressure, lb_f/ft^2;
$\dot{Q}$ = heat source, Btu/s;
$\dot{q}$ = heat transfer rate, Btu/s;
R = gas constant, lb_f-ft/lb-R;
r = radius, ft;
$\dot{S}$ = heat source, Btu/s;
S = momentum source, lb;
T = temperature, °F;
t = time, s;
V = volume, ft^3;
v = fluid velocity, ft/s;
z = compressibility factor;
δ = tube wall characteristic length, ft;
ε = surface roughness of pipe, ft;
ρ = density, lb/ft^3; and
ϕ = specific volume, specific heat, or viscosity.

Subscripts
f = liquid state;
g = vapor state;
i = ith node;
ij = branch connecting nodes i and j;
j = jth node;
s = solid node;
sa = solid to ambient;
sf = solid to fluid;
ss = solid to solid; and
u = upstream.

1. Introduction

Dynamics of propellant feedline is a complex process that may involve coupled two-phase flow and fluid-structure dynamics with heat transfer. As the fluid flows through the feedline, complex transients develop such as pressure surges and pressure oscillations due to sudden control valve operations. In cryogenic propulsion systems, feedline experience

very large temperature gradient and solid wall heat conduction interacts with flow convection and vice-versa. As the liquid propellant travels from the tank to the turbo pump, as soon as it makes initial contact with pipe, it turns into vapor because of the rise in temperature. As the pipe is cooled, the vapor becomes a mixture of vapor and liquid before it returns to a full liquid. Because of change in fluid density, the average velocities are significantly higher in the vapor region of the tube. Modeling these coupled two-phase flow dynamics and convection heat transfer and understanding how they affect heat transfer from the tube wall to the flowing cryogen are important for high mass and chilldown time efficiencies. Apart from cryogenic applications, feedline dynamics is also a crucial component of many industrial facilities such as hydraulic power plants and drainage systems in which flow control valves cause high-pressure developments. Often pipeline filled with liquid entrap air causing further increase in amplitude and frequency of pressure.

There have been several analytical and experimental investigations into chill down of cryogenic transfer line. Chill down of LN_2 flow in vertical and horizontal tubes was investigated experimentally by Antar and Collins (1997) and Yuan *et al.* (2007), respectively. In Van Dresar *et al.*'s study (2002), heat transfer and flow regimes of hydrogen and nitrogen were reported for a small-scale cryogenic transfer line. In Cross *et al.*'s study (2002), a computational study of cryogenic feedline was presented neglecting fluid transients. In Majumdar and Ravindran's study (2011), cryogenic feedline chill down problem including fluid transients was studied and concluded that increasing the driving pressure and providing sub-cooling decreases the chill down time. The problem of pressure surges in propulsion feedline with entrapped air in liquid carrier has also been investigated by many researchers. In Prickett *et al.*'s study (1992), a series of experimental studies were reported on tests to determine the effects of water hammer in pipe networks. In Lin and Bakers study (1995), testing conducted in the feed system priming process was reported. In Zhou *et al.*'s study (2002), experimental measurements of pressure inside pipeline with entrapped air were reported. They showed entrapped air functions as a cushion and decreased the maximum air pressure.

In the present study, an adaptive unstructured finite volume procedure for the prediction of complex coupled transients in fluid network is presented. In the past, most of the developments in network solver were in unstructured finite volume procedures for spatial discretization of flow network with branching. In this network model reduction approach, the fluid region is partitioned into a series of discrete nodes connected by branches and solid region is partitioned into a series of solid nodes connected by solid-to-solid conductors. In coupled fluid-structure problems, the solid nodes are connected by fluid-to-solid conductors, which model convection from the fluid to the pipe wall, see Figure 1. Conservation equations

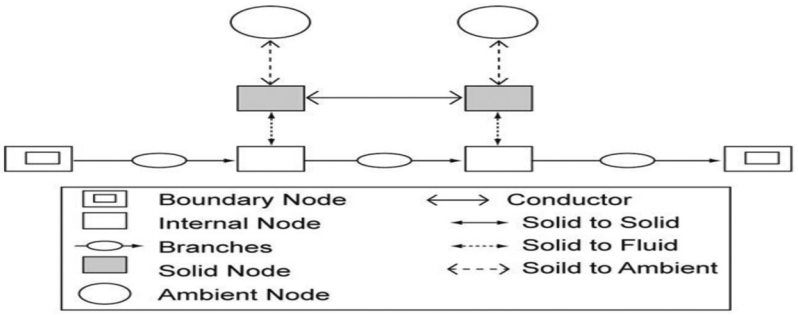

Figure 1.
Typical flow network consisting of fluid nodes, solid nodes, flow branches and conductors

are expressed in conservative unsteady finite volume form for fluid network. The conservation equations for scalar fields such as pressure, temperature and concentration of species are solved at the internal fluid nodes in conjunction with the thermodynamic equation of state, whereas momentum conservation is solved for mass flow rates at the branches. The conservation of energy for solid nodes is solved at the solid nodes for solid node temperature simultaneously with all the other fluid flow conservation equations. This way the reduced-order fluid network modeling provides a feasible approach to aerospace system modeling and analysis (Cross *et al.*, 2002; Majumdar and Ravindran, 2011; Majumdar and Steadman, 2001; Majumdar and Ravindran, 2010). Yet there are practical aerospace configurations for which large versions of flow circuit are needed resulting in higher dimensional reduced-order network models. Moreover, predicting complex transients such as thermo-fluid and fast-slow-fast transients in long-time simulations are still prohibitively expensive with these network models. Despite this, there has been no attempt at developing an adaptive capability for simulations in fluid network. It is important to note here that there has been a growing interest in adaptive time-stepping approaches for computational fluid dynamic analysis of fluid flow components (Turek, 1999; Volker and Rang, 2010; Berrone and Marro, 2009; Gao *et al.*, 2010; Gresho *et al.*, 2008). Regardless of the settings, one desired property of adaptive methods is efficiency. Most of the existing adaptive time-stepping schemes for computational fluid dynamics (Turek, 1999; Volker and Rang, 2010; Berrone and Marro, 2009; Gao *et al.*, 2010; Gresho *et al.*, 2008) are based on some type of error estimation by comparing the solutions computed with two different time-stepping schemes and thus suffer either from increase in computational cost or from stability restriction. The proposed adaptive approach methodology automatically adjusts the time-step via a feedback law of errors defined by normalized changes in key variables and does not suffer from these drawbacks. The proposed methodology has been implemented in the network flow simulation software GFSSP (Majumdar and Ravindran, 2011) to model experimental setups of a sudden valve opening in a water system with entrapped air (Lee and Martin, 1999; Lee, 2005) and to conjugate heat transfer in long cryogenic pipe line (Brennan *et al.*, 1966). The numerical results are compared with results obtained with existing time-stepping schemes and validated by comparing with the available experimental data.

2. Adaptive finite volume formulation of fluid network

The prediction of feedline dynamics involves numerically solving unsteady mass, momentum and energy conservation equations along with the equation of state. The conservation equations are written in conservative finite volume form for a flow network of internal nodes, boundary nodes and branches. Fluid enters the network through an inlet boundary node and exits through an outlet boundary node and at the boundary nodes, pressure and temperature are prescribed. A control volume is defined at each internal node and the boundaries of which are assumed to have inflow and outflow of mass and energy. Assuming that the flow is driven by the pressure differential between the upstream and downstream nodes, the scheme computes pressure from themass conservation equation and temperature from the energy conservation equation at the internal nodes in conjunction with the equation of state. Details of the governing equations and finite volume discretization are explained below.

2.1 Governing equations and finite volume formulation

2.1.1 Mass conservation equation. Pressure at internal node is calculated from the mass conservation equation. Figure 2 is a schematic showing adjacent nodes, their connectivity

and the indexing convention. The mass conservation equation at the ith node can be expressed as follows, and each term has the unit of pounds of mass per second:

$$\frac{(m_i)_{t_n+\Delta t_n} - (m_i)_{t_n}}{\Delta t_n} = -\sum_{j=1}^{N} \dot{m}_{ij} \tag{1}$$

Equation (1) shows that for transient flow, the net mass flow from a given node equals the rate of the change of mass in the control volume.

2.1.2 Energy conservation. The energy conservation equation for node i can be expressed following the first law of thermodynamics and using enthalpy as the dependent variable. It can be written as:

$$\frac{m\left(h - \frac{p}{\rho J}\right)_{t_n+\Delta t_n} - m\left(h - \frac{p}{\rho J}\right)_{t_n}}{\Delta t_n} = \sum_{j=1}^{N} \{\max[-\dot{m}_{ij}, 0]h_j - \max[\dot{m}_{ij}, 0]h_i\} + \dot{q}_{sf} \tag{2}$$

Equation (2) shows that for transient flow, the rate of increase of internal energy in the control volume is equal to the rate of energy transport into the control volume minus the rate of energy transport from the control volume plus any external rate of heat transfer from the solid node $(\dot{q}_{sf})$. The max operator used in equation (2) is known as an upwind differencing scheme and has been extensively used in the numerical solution of Navier–Stokes equations in convective heat transfer and fluid flow applications. When the flow direction is not known, this operator allows the transport of energy only from its upstream neighbor. In other words, the upstream neighbor influences its downstream neighbor but not vice versa.

2.1 3 Momentum conservation equation. The momentum conservation in equation (2) represents the balance of fluid forces acting on a given branch. The flow rate in a branch is calculated from this equation. A typical branch configuration is shown in Figure 3. Inertia, pressure and friction are considered in the conservation equation. It should also be noted that the flow rate, $\dot{m}_{ij}$, is a vector quantity. A negative value of $\dot{m}_{ij}$ signifies that the flow is directed from the jth node to the ith node:

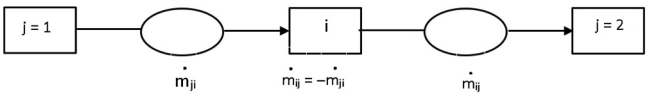

Figure 2.
Schematic of GFSSP nodes and branches in context of mass conservation equation for node i

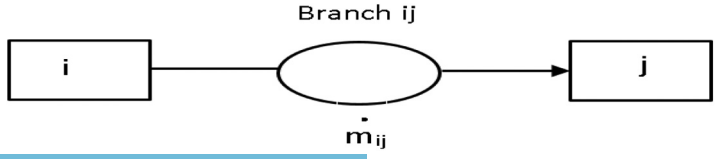

Figure 3.
Schematic of GFSSP nodes and branches in the context of momentum conservation equation for branch ij

$$\frac{(mu)_{t_n+\Delta t_n} - (mu)_{t_n}}{g_c \Delta t_n} = \max\left[-\dot{m}_{ij}, 0\right](u_d - u_{ij}) - \max\left[\dot{m}_{ij}, 0\right](u_{ij} - u_u) + (p_i - p_j)A_{ij} - K_{f^*}\dot{m}_{ij}|\dot{m}_{ij}|A_{ij} \quad (3)$$

The left-hand side of the equation represents the rate of the change of momentum with time. The first two terms on the right side of the momentum equation represent the inertia of the fluid. The second term is significant when there is a large change in area or density from branch to branch. The third term on the right side of the momentum equation represents the pressure gradient in the branch. The pressures are located at the upstream and downstream faces of a branch. The fourth term represents the frictional effect. Friction is modeled as a product of K_{f*}, the square of the flow rate and area. K_{f*} is a function of the fluid density in the branch and the nature of flow passage being modeled by the branch. To determine K_{f*}, for pipe flow, it is expressed as:

$$K_{f^*} = \frac{8f^*L}{\rho_u \pi^2 D^5 g_c}$$

where L is the pipe length, D is the pipe diameter and ρ_u is the density of the fluid at the upstream node of a given branch. The Darcy–Weisbach friction factor f^* in the definition of K_{f*} is calculated from the Colebrook (1939) equation, which is expressed as:

$$\frac{1}{f^*} = -2\log\left[\frac{\varepsilon}{3.7D} + \frac{2.51}{\mathrm{Re}\sqrt{f^*}}\right],$$

where ε/D is the surface roughness factor and Re (equal to $\rho\ UL/\mu$) is the Reynolds number. For flow through a restriction, K_{f*} is expressed as $K_{f*} = 1/2g_c\rho_u C_L{}^2A^2$ where C_L is the flow coefficient, A is the area of restriction and g_c is the conversion factor for engineering unit. It is assumed that the role of the flow coefficient C_L is independent of the flow direction. The density and viscosity for the Reynolds number are computed from quality, assuming homogeneous mixture, to account for two phase flow. The momentum conservation equation also requires knowledge of the density and the viscosity of the fluid within the branch. These are functions of the temperatures, and pressures, and can be computed using the thermodynamic property program by Hendricks *et al.* (1975) that provides the thermodynamic and transport properties for different fluids.

2.1.4 Equation of state for real fluid. Transient flow calculations require the knowledge of resident mass in a control volume. The resident mass in the ith control volume is calculated from the equation of state for real fluids:

$$m = \frac{pV}{RTz} \ . \quad (4)$$

The compressibility factor z and temperature T in equation (4) are calculated from the thermodynamic property program (Hendricks *et al.*, 1975) for a given pressure and enthalpy.

2.1.5 Phase change. Modeling phase change is fairly straightforward in the present formulation. The vapor quality of saturated liquid vapor mixture is calculated from:

$$x = \frac{h - h_f}{h_g - h_f} \ .$$

Assuming a homogeneous mixture of liquid and vapor, the density, specific heat and viscosity are computed from the following relations:

$$\varphi = (1-x)\phi_f + x\phi_g \ .$$

where φ represents specific volume, specific heat or viscosity.

2.1.6 Specie conservation equation. To model a homogeneous mixture of liquid and gas, the conservation equations for both liquid and gaseous species are solved in conjunction with equations (1), (3) and (4). For mixtures, the concentration of fluid specie must be determined so that the density may be calculated. The concentration for the kth specie at node i is:

$$\frac{(m_i c_{i,k})_{t_n+\Delta t_n} - (m_i c_{i,k})_{t_n}}{\Delta t_n} \sum_{j=1}^{j=n} \{MAX[-\dot{m}_{ij}, 0] c_{j,k} - MAX[\dot{m}_{ij}, 0] c_{i,k}\} \tag{5}$$

Unlike a single fluid, the energy equation for a gas–liquid mixture is expressed in terms of temperature instead of enthalpy. Moreover, it is assumed that the liquid and gas have the same temperature; however, specific heat of liquid and gas is evaluated from a thermodynamic property program (Berrone and Marro, 2009). The density, specific heat and viscosity of the mixture are then calculated.

2.1.7 Energy conservation equation for solid. In fluid–solid network for conjugate heat transfer, solid nodes, ambient nodes and conductors become part of the flow network. A typical flow network for conjugate heat transfer is shown in Figure 1. The energy conservation equation for the solid node is solved in conjunction with all other conservation equations. The energy conservation for solid node i can be expressed as:

$$\frac{\left(mC_p T_s^i\right)_{t_n+\Delta t_n} - \left(mC_p T_s^i\right)_{t_n}}{\Delta t_n} = \sum_{j_s=1}^{n_{ss}} \dot{q}_{ss} + \sum_{j_f=1}^{n_{sf}} \dot{q}_{sf} + \sum_{j_a=1}^{n_{sa}} \dot{q}_{sa} + \dot{S}_i \tag{6}$$

The left-hand side of the equation represents rate of change of temperature of the solid node, i. The right-hand side of the equation represents the heat transfer from the neighboring node and heat source or sink. The heat transfer from neighboring solid, fluid and ambient nodes can be expressed as follows:

$$\dot{q}_{ss} = k_{ij_s} A_{ij_s} / \delta_{ij_s} \left(T_s^{j_s} - T_s^i\right) \ , \tag{7a}$$

$$\dot{q}_{sf} = h_{ij_f} A_{ij_s} \left(T_f^{j_f} - T_s^i\right) \ , \tag{7b}$$

and

$$\dot{q}_{sa} = h_{ij_a} A_{ij_a} \left(T_a^{j_a} - T_s^i\right) \ . \tag{7c}$$

The heat transfer rate can be expressed as a product of conductance and temperature differential. The conductance for equations (7a)-(7c) is:

$$C_{ij_s} = \frac{k_{ij_s} A_{ij_s}}{\delta_{ij_s}}; \ \mathrm{C}_{ij_f} = h_{ij_f} A_{ij_f}; \ \mathrm{C}_{ij_a} = h_{ij_a} A_{ij_a} \ , \tag{7d}$$

where effective heat transfer coefficients for solid to fluid and solid to ambient nodes are expressed as:

$$h_{ij_a} = h_{c,ij_a} + h_{r,ij_a} \ ,$$

$$h_{r,ij_f} = \frac{\sigma\left[\left(T_f^{j_f}\right)^2 + \left(T_s^i\right)^2\right]\left[T_f^{j_f} + T_s^i\right]}{\frac{1}{\varepsilon_{ij,f}} + \frac{1}{\varepsilon_{ij,s}} - 1} \ ,$$

and

$$h_{r,ij_a} = \frac{\sigma\left[\left(T_f^{j_a}\right)^2 + \left(T_s^i\right)^2\right]\left[T_a^{j_a} + T_s^i\right]}{\frac{1}{\varepsilon_{ij,a}} + \frac{1}{\varepsilon_{ij,s}} - 1} \ .$$

For two-phase flow heat transfer coefficient specification, we will use the modified Miropoloski's correlation (Miropolski, 1963). Miropolskii's correlation provides modified Nusselt, Reynolds and Prandtl numbers based on the fluid mixture parameter Y and mass fraction x, where:

$$Nu = h_c D / k_v$$

where:

$$Nu = 0.023(Re_{mix})^{0.8}(Pr_v)^{0.4}(Y)$$

where:

$$Re_{\text{mix}} = \left(\frac{\rho u D}{\mu_g}\right)\left[x + \left(\frac{\rho_g}{\rho_1}\right)(1-x)\right], \ Pr_g = \left(\frac{C_p \mu_g}{k_g}\right), \quad \text{and}$$

$$Y = 1 - 0.1\left(\frac{\rho_g}{\rho_1} - 1\right)^{0.4}(1-x)^{0.4} .$$

The required thermodynamic and thermophysical properties in all conservation equations during iterative calculation are provided by the thermodynamic property programs GASP (Hendricks *et al.*, 1975) and WASP (Hendricks *et al.*, 1973). We note here that the use of Miropoloski's correlation assumes that nucleate boiling can be neglected. Its use in the cryogenic feedline chilldown problem discussed in the sequel is justified because due to large initial wall super heat, the total heat transfer is large compared to the amount of heat transfer during nucleate boiling. Moreover, the boiling curve passes through the nucleate boiling regime very quickly as the heat flux increases as peak heat flux is approached from minimum heat flux in film boiling.

The dynamics inside propellant feedline is a complex coupled interaction of flow convection and solid wall heat conduction and vice versa. Their accurate resolution poses many challenges to network modeling and simulation, such as a need for large circuit, implicit time stepping, complex nonlinearity, etc. To address these challenges, a partitioned approach that takes advantage of the weak coupling between flow and heat transfer is used. In this approach, the equations that are strongly coupled are solved together by Newton iteration, whereas the equations that are weakly coupled are solved together by fixed point iterations. While this approach leads to savings in computational time, it is still prohibitively expensive computationally to conduct systematic grid-convergence studies that are

necessary to provide confidence that the discretization errors are minimized and well understood.

2.2 Adaptive time-stepping strategy

In this section, we propose an adaptive time-stepping strategy for network flow models that combines change of the solution in two subsequent time steps and proportional-integral-derivative (PID) feedback control theory. As the PID controller relies only on measured process and not on the knowledge of underlying process, it is well suited for adaptive time-step determination. It uses normalized changes in key variables such as flow rate, pressure and temperature to compute the local errors e_n. The control is constructed such that it reduces the time step if the solution change is relatively large and increases it if the change is small. If the error is larger than a given tolerance, this error signal will be sent to the PID controller, and the controller computes both the derivative and the integral of this error signal. The time step Δt to the flow solver is equal to the proportional gain (K_p) times the magnitude of the error plus the integral gain (K_i) times the integral of the error plus the derivative gain (K_d) times the derivative of the error. Let $e^{\dot{m}}$, e^p, e^h be the relative changes in time t_n of nodal flow rate, pressure and enthalpy are defined by:

$$e^{\dot{m}} = \hat{e}^{\dot{m}}/tol_{\dot{m}}, \qquad \hat{e}^{\dot{m}} = \|\dot{m}_n - \dot{m}_{n-1}\|/\|\dot{m}_n\|$$

$$e^p = \hat{e}^p/tol_p, \qquad \hat{e}^p = \|p_n - p_{n-1}\|/\|p_n\|$$

$$e^h = \hat{e}^h/tol_h, \qquad \hat{e}^h = \|h_n - h_{n-1}\|/\|h_n\|$$

and set

$$e_n = \max\left(e^{\dot{m}}, e^p, e^h\right) \tag{8}$$

where $tol_{\dot{m}}$, tol_p, tol_h are user-specified tolerances corresponding to the normalized changes in flow rate, pressure and enthalpy, respectively, and the norm used is the maximum norm defined by $\|p\| = \max_i p_i$. Then the PID feedback control yields the feedback gain:

$$G = \left(\frac{e_{n-1}}{e_n}\right)^{\frac{k_P}{(k+1)}} \left(\frac{1}{e_n}\right)^{\frac{k_I}{(k+1)}} \left(\frac{{e_{n-1}}^2}{e_n e_{n-2}}\right)^{\frac{k_D}{(k+1)}} \tag{9}$$

and

$$\Delta t^* = G\Delta t^n \tag{10}$$

See Gustafsson *et al.*'s study (1998), where G is the feedback gain factor and the constants k_P, k_I and k_D are the proportional, integral and derivative gains, respectively. Moreover, $k = 1$ for first-order-in-time time-stepping scheme and $k = 2$ for second-order-in-time time-stepping scheme. The parameter *tol* determines the required accuracy of the numerical solution. The extra computational cost in computing the new time-step Δt_{n+1} by this approach is negligible as it involves storing a few extra vectors and computing few norms. To avoid too large and too small time-step sizes, we introduce upper bound and lower bound

and allow the adaptive time step to vary only between two time-step limiters Δt_{min} and Δt_{max}. To avoid too large or too small values of gain factor G, we similarly introduce gain size limiters G_{max} and G_{min} such that $G_{min} \leq G \leq G_{max}$. In algorithmic form, the computation of the variable time step using this approach becomes the following: For time instance t_n, $n = 1, 2, 3 \ldots\ldots\ldots$, we shall proceed as follows:

Algorithm III.1

Input: $\dot{m}_n$, p, h, Δt_{min}, Δt_{max}, k_p, k_I, k_D, $tol_{\dot{m}_n}$, tol_p, tol_h, G_{max}, G_m

i. Initialize variables: $e_{n-2} = 1.d0$, $e_{n-1} = 1.d0$, $\Delta t_n = \Delta t_{min}$

ii. Compute e_n *using (8)*

iii. If $e_n > tol$. *reject the time step:*

a) $t_{n+1} = t_n - \Delta t$

b) $\Delta t_{n+1} = max((tol./e_n)\Delta t_n, \Delta t_{min})$

else

c) Compute G^* *using (9)*

d) Set $G = max(G^*, G_{min})$ *and* $G = min(G^*, G_{max})$

e) Compute Δt^* *using (10)*

f) Set $\Delta t = max(\Delta t^*, \Delta t_{min})$ *and* $\Delta t = min(\Delta t^*, \Delta t_{max})$

g) Set $\Delta t_{n+1} = \Delta t$.

To verify the robustness of the algorithm, we performed parametric studies for different PID feedback gain values k_p, k_I, k_D for the two problems. The algorithm was found to be robust with fewer time-step rejection when $k_p = 0.525$, $k_I = 0.2625$, $k_D = 0.03$, and used for all the numerical evaluations performed below. These studies also indicated that suitable values for *tol* depend on the order of the time discretization scheme and best results were found when $tol_j = 10^{-1}$.

3. Results and discussion

In this section, we evaluate the proposed adaptive unstructured finite volume approach for flow network by numerically solving first a fluid transient problem of entrapped air in water pipe and then solving a thermo-fluid transient problem of chilldown of cryogenic feedline.

3.1 Problem I: water pipe with entrapped air

A long pipe is attached to a reservoir containing liquid water at one end and closed at the other end. A ball valve separates the liquid water and entrapped air regions in the pipe, see Figure 4 (top). The controlling parameters such as the dimension of the pipeline, reservoir air column, are taken to be same as the experimental data from the studies of Lee and Martin (1999) and Lee (2005). The ball valve is opened from 0 per cent opening to a 100 per cent

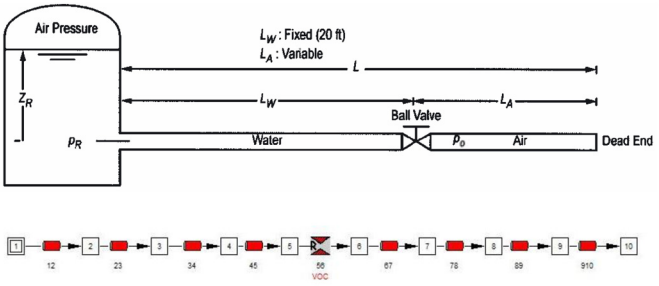

Figure 4.
Schematic of water pipe with entrapped air (Lee, 2005) (top) and a ten-node GFSSP model (bottom)

opening by controlling the angle of the ball valve. It starts opening at about 0.15 s and opens 100 per cent in about 4 s. The reservoir pressure and initial pressure of entrapped air are taken to be 102.9 psia and 14.7 psia, respectively, so that the ratio of the reservoir pressure to the initial pressure $P_R = 7$. The initial length for the water volume in the pipe L_l is fixed to 20 feet and the initial length of the air column in the pipe L_g is taken to be 16.23 feet so that the ratio of the initial length of the entrapped air column to the total length of the pipe α ($=L_g/L_T$) = 0.448. The pipe diameter is 1.025 in. The entrapped air and water are initially at 14.7 psia and 60°F, respectively. The computational domain has been divided into ten nodes, see Figure 4.

First, a grid independence study was conducted to establish computational accuracy with respect to spatial discretization. The flow domain was divided into grids consisting of 10 pipe segments, 20 pipe segments and 40 pipe segments with constant refinement ratio. The computed results showed that results did not change appreciably when the number of pipe segments was doubled. The reference solution is obtained by using a small constant time step $\Delta t = 0.005$ s. The proposed adaptive time-stepping algorithm is also tested with this initial time step. This selection allows convergence of the nonlinear solver (fixed point and Newton iteration) at the beginning of the process. Figure 5 shows the computed results for transient pressure at the pipe end (pressure at node 10). As can be seen from Figure 5, numerical results using the adaptive time-stepping scheme match quite well with those of the fixed time-stepping scheme. There is discrepancy between the numerical results and experimental results. This is mainly due to the assumption of a fully developed steady flow friction factor. According to Astleford *et al.* (1973), the discrepancy can also be attributed to compliance due to dissolved gas and bubbles in the feedline.

For the adaptive scheme, the time step is allowed to adjust between $\Delta t_{min} = 0.001$ and $\Delta t_{max} = 0.01$. The time history for the time step is presented in Figure 7 (left). While the flow variables such as pressure varies sharply, the time step is shortened to the minimum value of Δt_{min} and while the pressure varies mildly, the time step is increased back to Δt_{max}.

Our numerical experiments indicate that while both time-step-size limiters Δt_{max} and Δt_{min} are important for crucial for the adaptive method's efficiency and robustness, the value of Δt_{max} affects its performance more. As expected, it affects the CPU time and the total number of time steps needed to complete the simulations. Figure 6 shows the CPU time, total number of time steps and the total number of nonlinear iterations. It shows that as Δt_{max} increases in the adaptine scheme, not only the CPU time and the total number of time steps but also the total number of nonlinear iterations (Newton/fixed point iteration) decrease. With fixed time step, the nonlinear solver took a total of 90,473 iterations but with

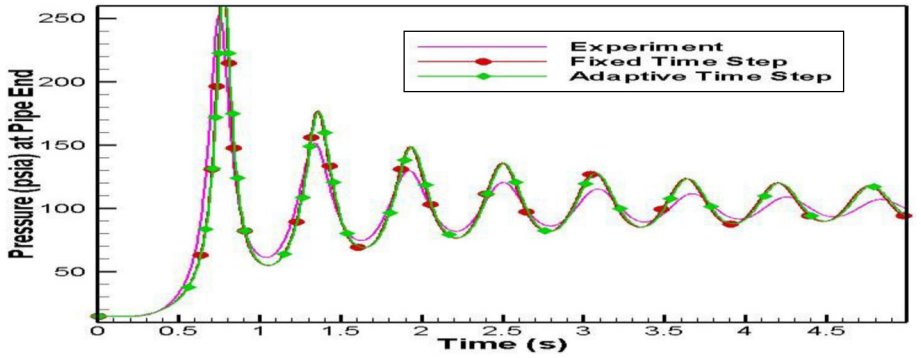

Figure 5.
Predicted air pressure using adaptive time-step, fixed time step and experimental data

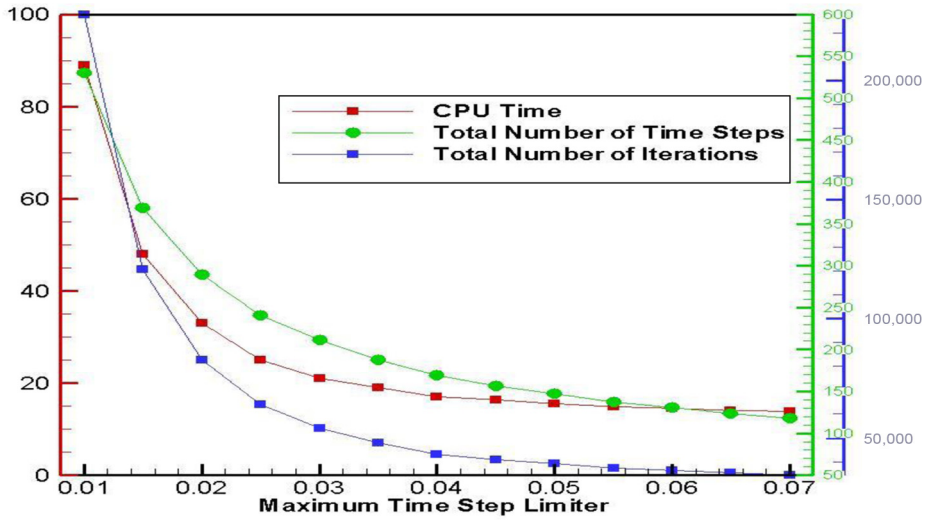

Figure 6.
Effect of time-step limiter Δt_{max} on CPU time, time steps and iterations

the adaptive method, it took a total of only 54,124 iterations. Figure 7 (right) compares the total number of nonlinear iterations taken at each time step by fixed time-step simulations and adaptive time-step simulation. As can be seen, adaptive algorithm clearly takes fewer nonlinear iterations at each time step.

However, there seems to be a critical Δt_{max} value beyond which increasing Δt_{max} does not translate into savings in computational effort. Our numerical experiments show that if Δt_{max} is too large, the algorithm may lead to too many time-step rejections or inaccurate results. In Figure 8, time history of pressure computed with adaptive time-stepping algorithm is shown for three different Δt_{max} values. The results clearly show that the accuracy of the results deteriorate for too large a Δt_{max} as evidenced by the good comparison with the experimental data. Our numerical experiments also show that if Δt_{max} is too large, the number of nonlinear iterations taken were kept equal to the maximum total iterations $Iter_{max}$ allowed in each time step.

To study the scalability of adaptive scheme's computational efficiency, a grid resolution investigation was carried out. Four meshes described in the first column of Table I were generated. In Table I, we also compare the computational effort to calculate the solution with

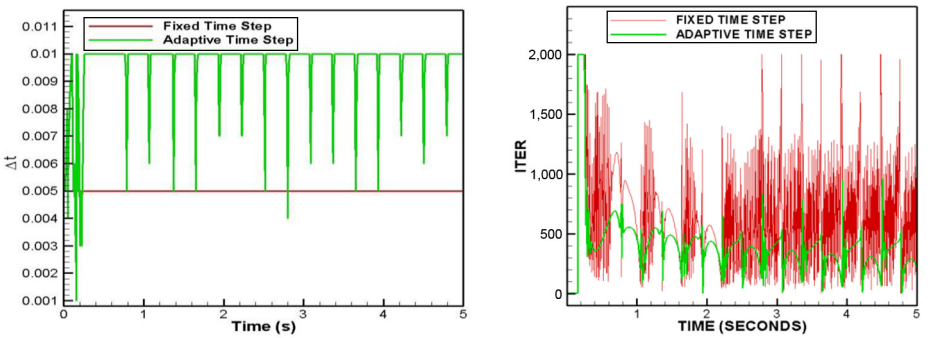

Figure 7.
Temporal evolution of time-step (left) and nonlinear iterations (right) as a function of time

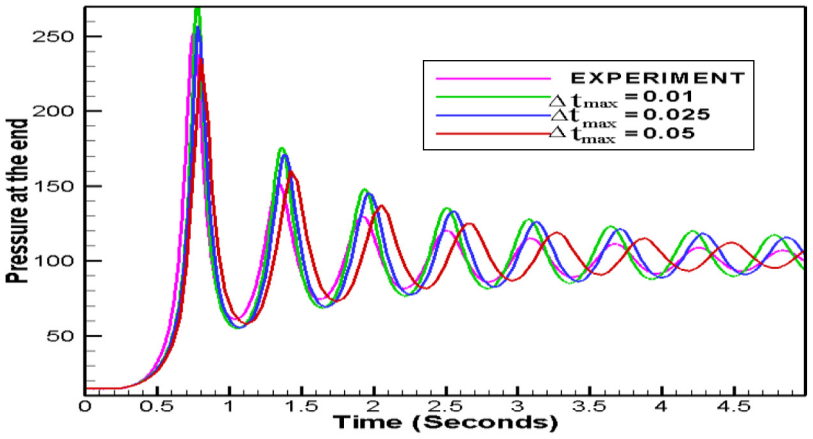

Figure 8. Transient pressure at the end of the pipe for various values of Δt_{max}

No. of nodes	CPU time (seconds) Adaptive time step	Fixed time step
10	25	251
20	81	785
40	315	3,297
80	1,605	17,673

Table I. CPU time comparison for Problem I

constant time step and adaptive time step. CPU times for simulations with different number of nodes (different number of pipe segments) are compared in second and third columns of Table I. The results there confirm that in all four cases, the computation time was decreased by about 90 per cent.

3.2 Problem II: chilldown of a cryogenic feedline

In this problem, we evaluate the adaptive approach in prediction of chill down of cryogenic feedline by using it to model the experimental setup of Brennan *et al.* (1966). A long pipe is attached to a storage dewar containing liquid hydrogen (LH_2) at one end, and it is open to the atmosphere, as shown in Figure 9 (top). It shows a schematic of the experimental setup used by Brennan *et al.* (1966), which consists of a 200-feet long and 0.625-in. inside diameter copper tube. The liquid hydrogen inside the tank was quickly pressurized from saturation temperature at atmospheric pressure (subcooled). At Time 0, a valve upstream of the pipe begins to open and LH_2 begins to flow into the feedline due to tank pressure

The simulations, reported below, used LH_2 supplied from the tank at 111.69 psia and at −424.57°F and exiting to the atmosphere at 12.05 psia. In the absence of experimental data, a 0.5-s transient valve opening was assumed. The entire domain is split into a set of finite volume with a number of segments, as shown in Figure 9 (bottom). The model consists of ten fluid nodes (two boundary nodes and eight internal nodes), eight solid nodes and nine branches. The upstream boundary node represents the LH_2 tank, while the downstream boundary node represents the ambient. The first branch represents the valve and the next eight branches represent the pipe. The first branch represents the valve and the next eight branches represent the pipe.

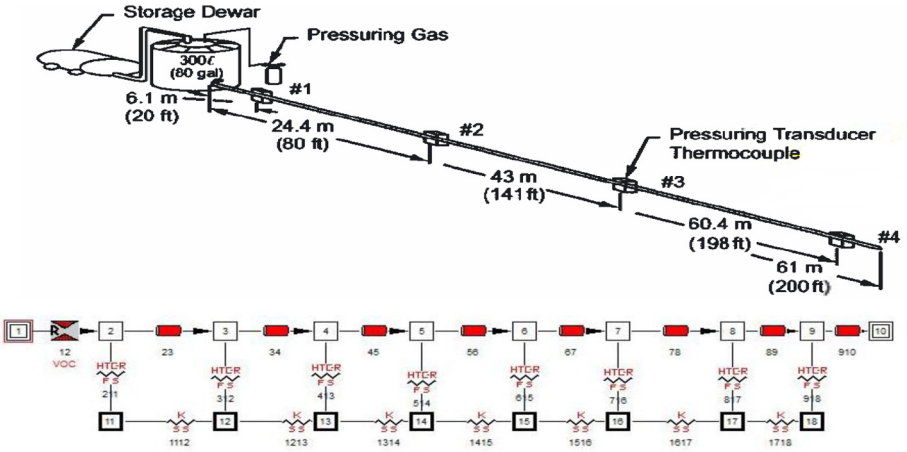

Figure 9.
Schematic of cryogenic feedline experimental setup (Brennan *et al.*, 1966) (top) and GFSSP model (bottom)

First, a grid independence study and a time-step independence study have been conducted to establish computational accuracy. The computation domain, as illustrated in Figure 9, has been divided into 10 pipe segments, 20 pipe segments, 40 pipe segments and 80 pipe segments.

The solid nodes are connected to the fluid nodes by fluid to solid conductors, which model convection from the fluid to the pipe wall. The modified Miropolskii's correlation (Miropolski, 1963) is used to calculate the convection coefficient for the two-phase flow. Because the pipe is vacuum jacketed copper transfer line, radiative heat transfer and heat transfer between the pipe walls and the ambient are assumed negligible. At the internal fluid nodes and branches, mass, momentum and energy equations are solved in conjunction with the thermodynamic equation of state to compute the pressures, flow rates, temperatures, densities and other thermodynamic and thermophysical properties. The heat transfer in the wall is modeled using the lumped parameter method, assuming the wall radial temperature gradient is small. At the internal solid nodes, the energy equation is solved in conjunction with all other conservation equations.

The reference results are calculated with constant time step $\Delta t = 0.001$s. The predicted temperature history is shown in Figure 10. Stations 1-4 are nodes whose locations correspond to four measurement locations in the experimental data. These stations are located at 20, 80, 140 and 200 feet, respectively, downstream of the tank.

These numerical predictions compare well to the measured temperatures. At this driving pressure, the pipe line chills down in about 46 s. Small discrepancy exists between prediction and experiments. This is partly due to coarseness of the network node – both solid and fluid – and partly due to the heat transfer coefficient that affects the longitudinal conduction that can be seen by noting that the discrepancy increases at each successive station in the downstream. As can be seen in Figure 10, the numerical model tends to slightly over predict the cooldown times. Likely reasons for computational results not matching experimental results are:

- inaccuracy of Miropolski's heat transfer correlation;
- representation of friction factor in two-phase flow assuming homogeneous mixture; and
- uncertainty in the experimental data being compared with.

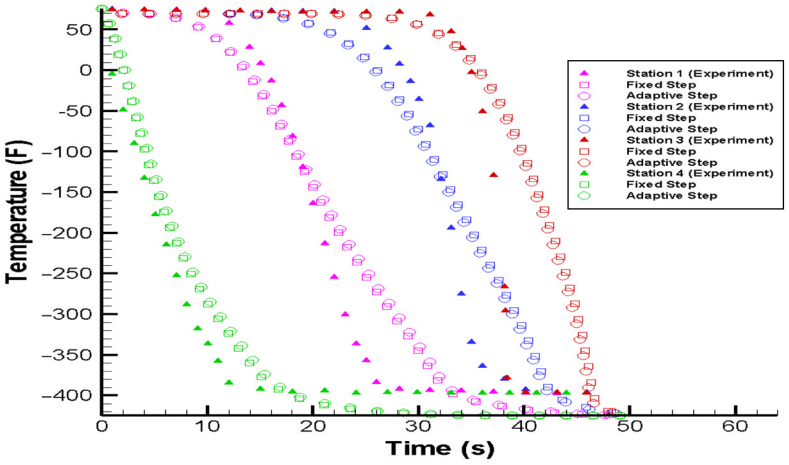

Figure 10. Transient temperature for subcooled LH2 for the driving pressures 111.69 psia at four stations

The adaptive time-stepping algorithm is tested with this problem by using an initial time step of $\Delta t = 0.001$ s. The time step is adjusted between $\Delta t_{min} = 0.001$ s and $\Delta t_{max} = 0.007$ s. The time history for the time step is presented in Figure 11. Figure 10 compares the wall temperatures of the adaptive time step predictions of the numerical model and the fixed time-step predictions over the course of a 100-s simulation. When the time step is adjusted

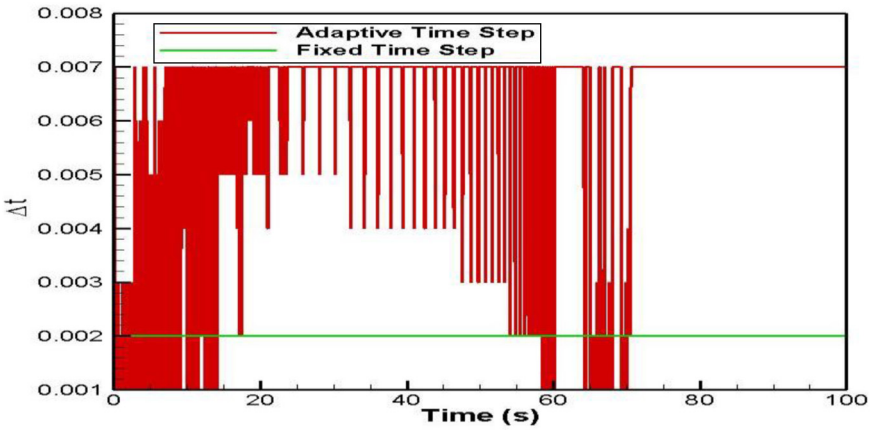

Figure 11. Temporal evolution of time-step variation as a function of time

No. of nodes	CPU time (seconds) Adaptive time step	Fixed time step
10	7,531	23,534
20	15,168	47,680
40	30,222	93,278
80	61,210	191,587

Table II. CPU time comparison for Problem II

according to the adaptive algorithm between Δt_{min} = 0.001 s and Δt_{max} = 0.007 s, the accuracy of the results is as good as with constant time step Δt = 0.002 s. When the fluid touches the warm pipe walls, heat transfer causes the liquid hydrogen to boil and the pipe wall temperature to rapidly decrease and the time step is shortened by the adaptive scheme. As the pipe chills down to the liquid temperature, the time step is increased back to Δt_{max} = 0.007s. CPU times for simulations with different number of nodes and constant time step are compared with CPU times for adaptive time-step simulations in Table II. In this problem, the adaptive scheme provides about 65 per cent decrease in CPU time for all the grid sizes considered. Moreover, adaptive time stepping reduced the number of nonlinear iterations needed to obtain the solution. With an increased time step, the chilldown time prediction becomes more inaccurate. When the time step is adjusted according to the adaptive algorithm between Δt_{min} = 0.001 s and Δt_{max} = 0.007s, the accuracy of the results is as good as with a constant time step of Δt = 0.001 s. Yet the computation time step is almost as short as with a constant time step of 0.007 s. This proves that the time adaptive technique we have presented is an effective tool to obtain accurate and economical network flow solutions of the rocket propulsion system problems.

4. Conclusions

An adaptive unstructured finite volume approach for efficient prediction of feedline dynamics in fluid network was presented. It represents a first attempt at applying the adaptive techniques of control theory used in the lumped parameter system case to the network fluid modeling case. In this approach, conservation equations were solved using unsteady finite volume approach with variable time step adjusted via a feedback strategy. The feedback strategy is based on errors defined by changes in key variables in two successive time instances. The ability to efficiently predict the coupled interactions in feedline was demonstrated by numerically solving first an air–water two-phase problem of entrapped air in water pipe and then solving a vapor–liquid two-phase problem of chilldown of cryogenic feedline. Numerical predictions with the adaptive strategy were compared with experimental data and found to be in good agreement. The strategy was found to be efficient for predicting feedline dynamics in flow network at reduced CPU time compared to traditional flow network solvers. Moreover, it was shown that the adaptive approach improves the convergence behavior of the nonlinear solvers leading to further reduction in CPU time. In the presented cases of entrapped air in water pipe and chilldown of cryogenic feedline, the CPU time was decreased about 90 and 68 per cent, respectively, without significant differences in the result.

References

Antar, B.N. and Collins, F.G. (1977), "Flow boiling during quenching in low gravity environment," *International Journal of Microgravity Science and Technology*, Vol. 3, pp. 18-128.

Astleford, W.J., Holster, J.L. and Gerlach, C.R. (1973), "Analysis of propellant feedline dynamics", NASA TR-NAS8-25919

Berrone, S. and Marro, M. (2009), "Space–time adaptive simulations for unsteady Navier – Stokes problems", *Computers and Fluids*, Vol. 38 No. 6, pp. 1132-1144.

Brennan, J.A., Brentari, E.G., Smith, R.V. and Steward, W.G. (1966), "Cooldown of cryogenic transfer lines – an experimental report", National Bureau of Standards Report, 9264, November.

Colebrook, C.F. (1939), "Turbulent flow in pipes, with particular reference to the transition region between smooth and rough pipe laws", *Journal of the Institution of Civil Engineers*, Vol. 11, pp. 133-156.

Cross, M.F., Majumdar, A.K., Bennett, J.C., Jr and Malla, R.B. (2002), "Modeling of chill down in cryogenic transfer lines", *Journal of Spacecraft and Rockets*, Vol. 39 No. 2, pp. 284-289.

Gao, Z., Vassalos, D. and Gao, Q. (2010), "Numerical simulation of water flooding into a damaged vessel's compartment by volume of fluid method", *Journal of Ocean Engineering and Science*, Vol. 37 No. 16, pp. 1428-1442.

Gresho, P.M., Griffiths, D.F. and Silvester, D.J. (2008), "Adaptive time-stepping for incompressible flow. I. Scalar advection-diffusion", *SIAM Journal on Scientific Computing*, Vol. 30 No. 4, pp. 2018-2054.

Gustafsson, K., Lundh, M. and Soderlind, G. (1998), "A PI step-size control for the numerical solution for ordinary differential equations", *BIT*, Vol. 28 No. 2, pp. 270-287.

Hendricks, R.C., Baron, A.K. and Peller, I.C. (1975), "GASP – a computer code for calculating the thermodynamic and transport properties for ten fluids: para hydrogen, Helium, Neon, Methane, Nitrogen, Carbon Monoxide, Oxygen, Fluorine, Argon, and Carbon Dioxide", NASA TND-7808, February.

Hendricks, R.C., Peller, I.C. and Baron, A.K. (1973), "WASP – a flexible fortran IV computer code for calculating water and steam properties", NASA TN-D-7391.

Lee, N.H. (2005), "Effect of pressurization and expulsion of entrapped air in pipelines", Ph.D. Thesis, Georgia Inst. of Technology, Atlanta.

Lee, N.H. and Martin, C.S. (1999), "Experimental and analytical investigation of entrapped air in a horizontal pipe", *Proceedings of the 3rd ASME/JSME Joint Fluids Engineering Conference, American Soc. Of Mechanical Engineers, Fairfield, NJ*, July, pp. 1-8.

Lin, T.Y. and Baker, D. (1995), "Analysis and testing of propellant feed system priming process", *Journal of Propulsion and Power*, Vol. 11 No. 3, pp. 505-512.

Majumdar, A.K. and Ravindran, S.S. (2010), "Computational modeling of fluid and thermal transients for rocket propulsion systems by fast nonlinear network solver", *International Journal of Numerical Methods for Heat and Fluid Flow*, Vol. 20 No. 6, pp. 617-637.

Majumdar, A.K. and Ravindran, S.S. (2011), "Numerical modeling of conjugate heat transfer in fluid network", *Journal of Propulsion and Power*, Vol. 27 No. 3, pp. 620-630.

Majumdar, A.K. and Steadman, T., (2001), "Numerical modeling of pressurization of a propellant tank", *Journal of Propulsion and Power*, Vol. 17 No. 2, pp. 385-390.

Miropolski, Z.L. (1963), "Heat transfer in film boiling of a steam-water mixture in steam generating tubes", *Teploenergetika*, Vol. 10 No. 5, pp. 49-52.

Prickett, R.P., Mayer, E. and Hermel, J. (1992), "Water hammer in a spacecraft propellant feed system", *Journal of Propulsion and Power*, Vol. 8 No. 3, pp. 592-597.

Turek, S. (1999), "Efficient solvers for incompressible flow problems: an algorithmic and computational approach", *Lecture Notes in Computational Science and Engineering*, Vol. 6, Springer.

Van Dresar, N.T., Siegwarth, J.D. and Hasan, M.M. (2002), "Convective heat transfer coefficients for near-horizontal two-phase flow of nitrogen and hydrogen at low mass and heat flux", *Cryogenics*, Vol. 41 Nos 11/12, pp. 805-811.

Volker, J. and Rang, J. (2010), "Adaptive time step control for the incompressible Navier – Stokes equations", *Computer Methods in Applied Mechanics and Engineering*, Vol. 199 Nos 9/12, pp. 514-524.

Yuan, K., Ji, Y. and Chung, J.N. (2007), "Cryogenic chilldown process under low flow rates", *International Journal of Heat and Mass Transfer*, Vol. 50 Nos 19/20, pp. 4011-4022.

Zhou, F., Hicks, F.E. and Steffler, P.M. (2002), "Transient flow in a rapidly filling horizontal pipe containing trapped air", *Journal of Hydraulic Engineering*, Vol. 128 No. 6, pp. 625-634.

Corresponding author
Sivaguru S. Ravindran can be contacted at: ravinds@uah.edu